AIP | Physics of Fluids

Multiple states of finger propagation in partially occluded tubes

A. L. Hazel, M. Pailha, S. J. Cox, and A. Juel

Citation: Phys. Fluids **25**, 062106 (2013); doi: 10.1063/1.4811176
View online: http://dx.doi.org/10.1063/1.4811176
View Table of Contents: http://pof.aip.org/resource/1/PHFLE6/v25/i6
Published by the AIP Publishing LLC.

Additional information on Phys. Fluids

Journal Homepage: http://pof.aip.org/
Journal Information: http://pof.aip.org/about/about_the_journal
Top downloads: http://pof.aip.org/features/most_downloaded
Information for Authors: http://pof.aip.org/authors

ADVERTISEMENT

PHYSICS OF FLUIDS **25**, 062106 (2013)

Multiple states of finger propagation in partially occluded tubes

A. L. Hazel,[1,a)] M. Pailha,[1,b)] S. J. Cox,[2] and A. Juel[1]
[1]*Manchester Centre for Nonlinear Dynamics and School of Mathematics, University of Manchester, Manchester M13 9PL, United Kingdom*
[2]*Institute of Mathematics and Physics, Aberystwyth University, Aberystwyth SY23 3BZ, United Kingdom*

(Received 21 August 2012; accepted 30 May 2013; published online 24 June 2013)

Recent experiments by Pailha *et al.* [Phys. Fluids **24**, 021702 (2012)] uncovered a rich array of propagation modes when air displaces oil from axially uniform tubes that have local variations in flow resistance within their cross-sections. The behaviour is particularly surprising because only a single, symmetric mode has been observed in tubes of regular cross-section, e.g., circular, elliptical, rectangular, and polygonal. In this paper, we present experimental results describing a new mode, an asymmetric localised air finger, that persists in the limit of zero propagation speed. We show that the experimental observations are consistent with a model based on capillary static calculations within the tube's cross-section, and the observed bistability is a consequence of the existence of multiple solutions to the Young–Laplace equations. The model also provides an upper bound for the previously reported symmetry-breaking bifurcation [A. de Lózar, A. Heap, F. Box, A. L. Hazel, and A. Juel, Phys. Fluids **21**, 101702 (2009)]. © *2013 AIP Publishing LLC*. [http://dx.doi.org/10.1063/1.4811176]

I. INTRODUCTION

The displacement of one fluid by another is a fundamental feature of two-phase fluid mechanics and underpins many industrial and natural processes, including mammalian breathing; the extraction of oil from porous media; coating processes; transport of multi-phase materials; and the manufacture of pharmaceuticals and comestibles. The canonical problem of air displacing an incompressible, Newtonian liquid has been extensively studied in simple rigid geometries, i.e., uniform tubes of circular,[1] rectangular, and elliptical[2] or polygonal cross-sections.[3] In these geometries, a single family of steadily propagating air fingers is found when the air is introduced at a constant flow rate. In applications, however, the geometry of the fluid-filled regions can be considerably more complex. For example, the pores in carbonate oil reservoirs are irregular and contain many regions of localised constriction;[4] and the airways of the lung experience significant local distortion via airway collapse or the accumulation of mucus.[5] Surprisingly, there are relatively few studies of simple two-phase displacement flows in more complex geometries, which motivates the present study.

We introduce an additional geometric length-scale by partially occluding tubes of rectangular cross-section with a centred rectangular block, thus introducing local variations in flow resistance across each tube, see Fig. 1. In contrast to the straightforward behaviour found in the simpler geometries, the presence of a partial occlusion can induce several distinct propagation states under constant flux forcing, including families of asymmetric[6] and oscillatory[7] air fingers. The selection of one state over another can dramatically change the volume of liquid extracted from the system, as well as alter the driving pressure gradient, so it is important to understand the origin and stability of the different states. In this paper, we report new experimental results demonstrating that bistable

a)Electronic mail: Andrew.Hazel@manchester.ac.uk
b)Present address: LOCIE, CNRS UMR 5271, Université de Savoie, Campus Scientifique, Savoie Technolac, 73376 Le Bourget du Lac Cedex, France.

 © 2013 AIP Publishing LLC

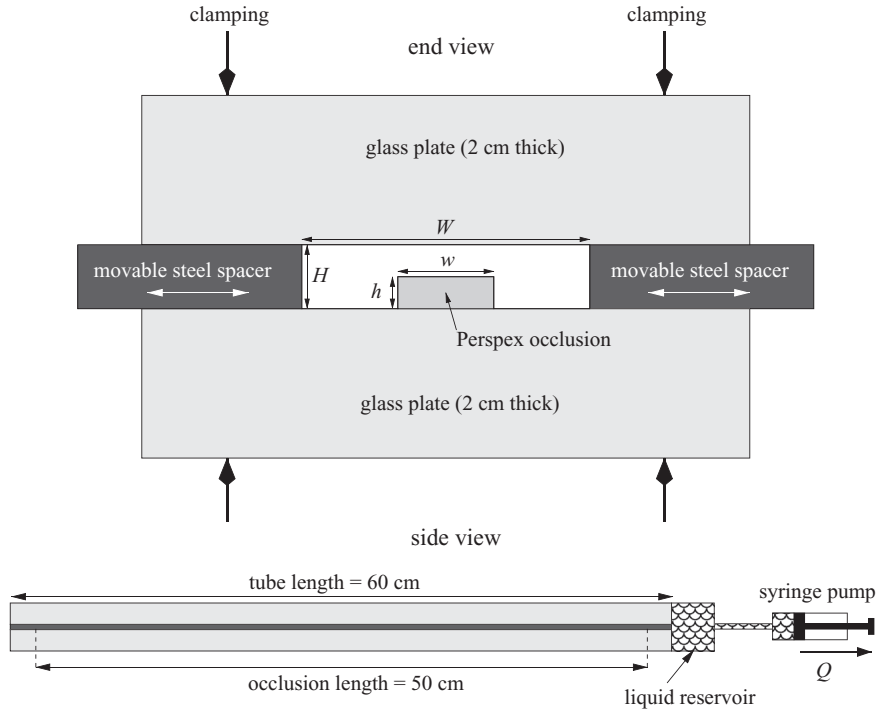

FIG. 1. Schematic diagram of the experimental setup. The end view shows the cross-section of the tube, which is rectangular with a centred step-change in depth. The dimensions of the cross-section of the flow tube are: $H = 3.07 \pm 0.01$ mm, $3 \leq W \leq 45$ mm, $w = 4.49 \pm 0.01$ mm, $h = 1.09 \pm 0.01$ mm or $h = 1.50 \pm 0.02$ mm. The side view illustrates how liquid is withdrawn at constant flow rate Q from one end of the initially liquid-filled tube, while the other end of the tube is open to the atmosphere.

behaviour can be observed at very low interface propagation speeds and propose a theoretical interpretation for the origin of the multiple observed propagation states.

The theoretical development exploits the experimental observations that for steadily-propagating fingers: (i) the liquid comes to rest soon after the passage of the finger tip; and (ii) the interface becomes axially uniform behind the tip. It follows that the finger cross-section behind the tip must approach a two-dimensional static equilibrium, whose shape depends on the propagation speed and is selected by an overall force balance on the air finger. For a static finger, the integrated component of surface tension acting normal to the tube axis must be balanced by the pressure jump integrated across the (projected) finger tip. The assumption of a hydrostatic pressure gradient in the liquid allows the cross-section to be determined without the need to compute the three-dimensional interface, see Refs. 8–10. For a moving finger, the flow of displaced liquid generates additional viscous stresses on the finger tip, which alter the force balance. The exact calculation of the viscous stresses for a given flow rate requires detailed resolution of the near-tip fluid flow, which can be achieved asymptotically for very small propagation speeds[10,11] or numerically by three-dimensional simulations.[2,6] Instead, however, we make use of the fact that the interface cross-section can be used as a proxy for the propagation speed. This theoretical route is motivated by the lack of available analytical solutions over the full range of propagation speeds and the challenges posed by numerical modelling in these partially occluded geometries, which stem from the need to resolve thinning liquid films as the propagation speed is reduced. We proceed to classify the different propagation states by their interface cross-sections and calculate the possible cross-sections for a number of tube geometries.

Using this approach, we demonstrate that for sufficiently high occlusions the system can be bistable even when the fluid is static: the finger is either symmetric or localised in one of the two side-channels. We investigate the existence of the localised fingers experimentally and examine their subsequent development with increasing flow rate. It is our contention that the multiple families

of propagating fingers observed in this system are all related to the occurrence of the symmetry breaking in the capillary statics and we find that the experimental results in the absence of flow are in quantitative agreement with theoretical predictions.

In Sec. II, we briefly describe the experimental apparatus, and the experimental results are presented in Sec. III. In Sec. IV, we quantify the theoretical approach and present results from the required capillary static simulations. In particular, we argue that the simulations can provide an upper bound for the location of the previously reported symmetry-breaking bifurcation[6] and hence provide insight into the physical origin of the changes in nature and location of the bifurcation with variations in geometry. Finally, in Sec. V we conclude with a summary and discussion of potential future applications to microfluidic devices.

II. EXPERIMENTAL SETUP

A schematic of the experimental apparatus is shown in Fig. 1. It is described in detail in Refs. 6 and 7 and thus we give only a brief description of the points pertinent to the present study.

The flow tube consisted of two horizontal, 60 cm long float-glass sheets separated by precision-machined stainless steel strips, so that the total height of the tube was $H = 3.07 \pm 0.01$ mm and its width W could be adjusted to yield aspect ratios $\alpha = W/H$ in the range $1 \leq \alpha \leq 15$. The tubes were uniform to better than 0.3% and 0.8% of their heights and widths, respectively.[12] An axially-uniform step-change in the height of the cross-section was achieved by positioning a 50 cm long rigid rectangular rod of width $w = 4.50 \pm 0.01$ mm symmetrically halfway across the bottom boundary of the tube (see Fig. 1). The occluding step was machined from Perspex to enable direct visualization and bonded to the glass boundary with double-sided tape. Two step heights were used, $h = 1.09 \pm 0.01$ and 1.50 ± 0.02 mm, giving two obstacle height ratios of $\alpha_h = h/H = 0.35$ and 0.49 while obstacle width ratios were in the range $1/8 \leq \alpha_w = w/W \leq 1/2$. The errors in the positional accuracy and axial uniformity of the obstacles were better than 0.5% and 3% of the occlusion width, respectively.

Initially, each tube was completely filled with silicone oil (Basildon Chemicals Ltd., with a density of $\rho = 961\,\mathrm{kg\,m^{-3}}$, a dynamic viscosity of $\mu = 5.4 \times 10^{-2}\,\mathrm{Pa\,s}$, and a surface tension of $\sigma = 2.1 \times 10^{-2}\,\mathrm{N\,m^{-1}}$). A two-phase displacement flow was induced by withdrawing liquid at a constant volumetric flow rate Q using a syringe pump (KDS210) connected to one end of the tube; the other end remained open to the atmosphere. A short (5 cm) unoccluded rectangular inlet section ensured that the finger was initially centred and symmetric about the mid-plane of the tube. The system rapidly adjusted to a new state after entering the partially occluded tube, and transients decayed over very short distances for all flow rates away from critical points. The motion of the steadily propagating finger tip was recorded from above by a video camera whose field of view covered the final 20 cm of the tube. The velocity of the finger tip, U, and hence capillary number, $Ca = \mu U/\sigma$, a dimensionless measure of the propagation speed, were determined from image analysis of the frames. Overview photos were also taken to characterize fingers in the entire tube with a high resolution (3872 × 2592 px) still camera. The experimental value of the Weber number, the ratio of inertial to surface tension forces, remains low ($We = \rho U^2 H/2\sigma < 0.04$), so inertial effects are negligible. However, the experimental value of the Bond number, the ratio of gravitational to surface tension forces, is $Bo = \rho g H^2/4\sigma = 1.058 \pm 0.007$, where g is the acceleration due to gravity; and so gravitational forces are not negligible in the experiments.

The localization of the propagating finger to the least constricted regions of the cross-section of the tube is quantified by a parameter $-0.5 < \delta < 0.5$, defined to be the offset from the middle of the finger to the middle of the tube, divided by the tube width, see inset in Fig. 2. This measure, which is only suitable for non-oscillatory fingers, was taken at a distance of 50 mm behind the finger tip once the finger had reached a constant width. δ is zero for fingers that propagate symmetrically about the vertical axial centre plane, and takes either positive or negative values for symmetry-broken states. A bulk measure of the fluid displacement is given by the wet fraction $m = 1 - Q/(AU)$, defined as the ratio of the liquid volume that remains once the finger has exited the tube to the total volume of the tube; here, $A = WH - wh$ is the cross-sectional area of the tube.

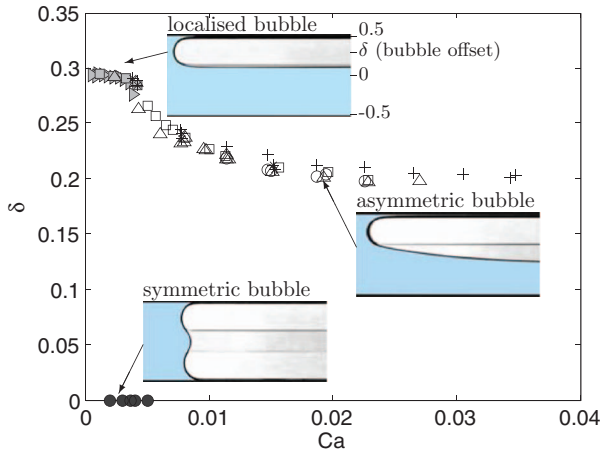

FIG. 2. Dependence of the finger tip offset from the tube centreline on Ca for $\alpha_w = 1/4$, $\alpha_h = 0.49$, and $\alpha = 6.0$. The value of the offset δ was measured 50 mm behind the finger tip, as shown schematically. Inset top-views are shown of the main finger types: symmetric (solid black symbols), asymmetric non-localised (white, $(*)$ and $(+)$ symbols), and localised state (solid light grey symbols). Both localised and symmetric fingers are stable for very low values of Ca. The symbols distinguish the perturbations applied to the propagating finger in order to reach the different states: $(\circ)$ experiments start from rest, $(\triangle)$ experiments start at a high flow rate that is then reduced. A localised finger was formed as a static initial condition $(\square)$ by driving a finger at high flow rate before interrupting the flow, and then restarting the experiment at the desired value of Ca. The other perturbations were applied by blocking parts of the cross-section over a short distance at the inlet of the tube: $(\triangleright)$ one side-channel and region over obstacle blocked, $(+)$ only region over obstacle blocked, or $(*)$ only one side-channel blocked.

III. EXPERIMENTAL RESULTS

A. Multiple families of propagating fingers and bi-stability at $Ca = 0$

We explored the range of different propagating fingers that could be selected experimentally by applying a variety of initial conditions and finite amplitude perturbations to the flow. Results are shown in Fig. 2 for $\alpha_w = 1/4$, $\alpha_h = 0.49$, and $\alpha = 6.0$, where the finger offset is shown as a function of Ca. We find three different states of finger propagation: symmetric (black symbols), asymmetric non-localised (white symbols, (*) and (+)), and asymmetric localised (grey symbols). A snapshot of each type of finger is inset into Fig. 2. A finger that is symmetric about the vertical axial midplane of the tube forms spontaneously at low Ca $(\bullet)$. A discontinuous transition to asymmetric non-localised fingers occurs at a critical value of Ca, and we refer to Ref. 6 for a discussion of the dependence of this bifurcation diagram on the geometric parameters α_w and α_h. We tested the stability of asymmetric non-localised fingers at values of Ca below the transition point by driving a finger at a large value of Ca for approximately 15 cm, before applying a step-change reduction in Ca (results denoted by $\triangle$ in Fig. 2). Other perturbations were applied by blocking parts of the cross-section over a short distance (of approximately 10 mm) at the inlet for the duration of the experiment. We either: (i) kept both side-channels open and blocked over the obstacle (denoted +); (ii) kept only one side-channel open and blocked over the obstacle (denoted $\triangleright$); or (iii) blocked only one side-channel and kept the region over the obstacle and the other side-channel open (denoted *). The asymmetric localised finger is confined to one of the side-channels within the constricted tube, and it is only selected for small values of Ca. We were also able to form such a localised finger as a static initial condition $(\square)$ by driving a finger at high flow rate before interrupting the flow, and then restarting the experiment at the desired value of Ca. In Fig. 2, the short branch of approximately constant (non-zero) offset values observed at low Ca corresponds to the localised fingers, which transition continuously to asymmetric non-localised fingers as Ca is increased. Moreover, their presence indicates that the flow is bistable over a range of small capillary numbers in our chosen geometry.

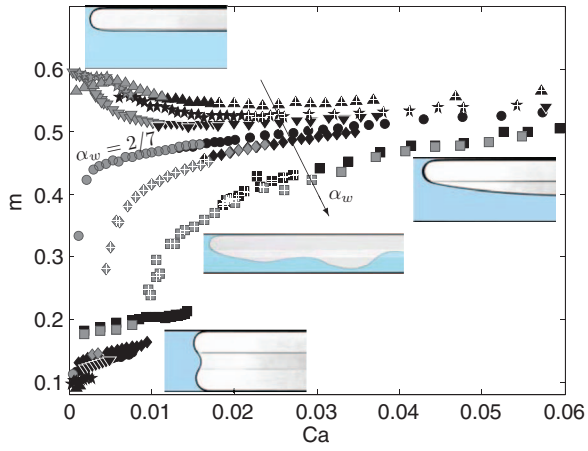

FIG. 3. Wet fraction m as a function of the capillary number Ca for $\alpha_h = 0.49$ and different values of α_w. Black markers: experiments start from rest; grey markers: experiments start at a high flow rate that is then reduced. Markers with a white cross correspond to an oscillatory state: (■) $\alpha_w = 2/5$, (♦) $\alpha_w = 1/3$, (●) $\alpha_w = 2/7$, (▼) $\alpha_w = 1/4$, (★) $\alpha_w = 1/5$, (▲) $\alpha_w = 1/8$. The arrow indicates the direction of increasing α_w and illustrative finger shapes are shown as insets. The data for $\alpha = 2/7$ are explicitly marked because it divides regions of different qualitative behaviour: for $\alpha < 2/7$, the system does not return to the symmetric state when Ca is reduced from an initially high flow rate. The data for $\alpha_w = 2/5$ and $\alpha_w = 1/3$ were previously presented in Ref. 7.

B. Bifurcation diagram and oscillatory fingers

The behaviour of the system for $\alpha_h = 0.49$ with different tube widths, $1/8 \leq \alpha_w \leq 2/5$, is shown in Fig. 3. Different initial conditions similar to those applied in Fig. 2 were used to reach the three main states of finger propagation, namely symmetric, asymmetric non-localised, and localised fingers. For all these values of α_w, the bifurcation from symmetric to asymmetric non-localised finger appears subcritical.

For $\alpha_w > 2/7$, Pailha *et al.*[7] proposed a global bifurcation scenario that involves the homoclinic connection of an asymmetric oscillatory solution (shown with white crosses in Fig. 3) to an unstable symmetry-broken state. In that case, the steady asymmetric non-localised finger is only observed for larger values of Ca beyond the range of the existence of the oscillatory finger, which Pailha *et al.*[7] conjectured to bifurcate from the steady asymmetric non-localised finger through a supercritical Hopf bifurcation as the parameter Ca decreases.

For $\alpha_w = 2/7$, the bifurcation from the symmetric finger is to a steady asymmetric non-localised finger, and for $\alpha_w < 2/7$, the asymmetric finger smoothly evolves towards a localised finger as Ca is reduced. In this case, oscillatory asymmetric fingers are not observed in the vicinity of the transition point, suggesting that the symmetric finger loses stability through a local subcritical symmetry-breaking bifurcation. In general, the value of m corresponding to the localised fingers decreases as Ca is increased from zero, apart from when $\alpha_w = 1/8$ and there is an initial increase for $Ca \approx 0$ to 0.005. As Ca increases further, the wet fraction reaches a minimum beyond which it increases monotonically with Ca. For both $\alpha_w = 2/7$ and $\alpha_w = 1/4$ (shown in Fig. 2), oscillatory fingers were not observed at all, but for the two widest tubes ($\alpha_w = 1/5$, $1/8$), oscillatory fingers were seen instead of steady asymmetric non-localised fingers for Ca above that corresponding to the minimum value of the wet fraction.

A comparison between oscillations in a wide tube ($\alpha_w = 1/8$) and a narrow tube ($\alpha_w = 1/3$) is shown in Fig. 4. These oscillations arise at widely different values of Ca, but the physical mechanism underlying the oscillations in both cases is associated with the local change in height of the tube's cross-section. As discussed in Ref. 7, when the edge of a widening finger passes sideways over the edge of the obstacle, there is a decrease in cross-sectional curvature as the interface expands into the unoccluded region. The induced local increase in pressure drives the oil away from the expanding interface (or bulge), which rapidly moves further sideways. The interface then reaches a quasi-equilibrium configuration where the change in axial curvature of the interface balances the

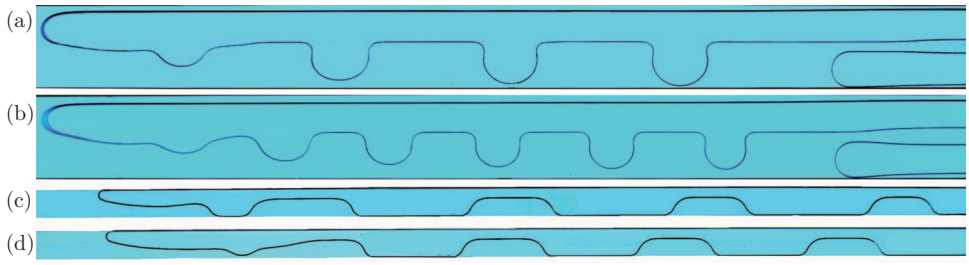

FIG. 4. Oscillatory pattern "shed" behind a finger propagating under constant flow rate from right to left for $\alpha_h = 0.49$: (a) $\alpha_w = 1/8$, $Ca = 3.69 \times 10^{-2}$, (b) $\alpha_w = 1/8$, $Ca \simeq 6.8 \times 10^{-2}$, (c) $\alpha_w = 1/3$, $Ca = 5.74 \times 10^{-3}$, (d) $\alpha_w = 1/3$, $Ca = 7.14 \times 10^{-3}$. The field of view is 400 mm long. Despite the occurrence of oscillations at very different values of Ca, the mechanism underlying their formation is similar in narrow and wide tubes. In particular, the spatial wavelength of the pattern decreases in both cases with increasing Ca, as discussed by Pailha *et al.*[7] in the case of narrow tubes. Figures 4(c) and 4(d) are reprinted with permission from Phys. Fluids **24**, 021702 (2012). Copyright 2011 American Institute of Physics.

change in cross-sectional curvature set by the geometry of the tube. The conditions for oscillations are not achieved until symmetry is lost, after which the edge of the finger crosses the obstacle beyond the rapid change in curvature associated with the tip region. In the narrow tube the interfacial bulge grows to reach the side wall of the tube before a quasi-equilibrium state is achieved, see Figs. 4(c) and 4(d). In the wide tube, the balance between axial and cross-sectional curvatures is reached before the interface reaches the side wall and the interface takes the form of a series of circular arcs when viewed from above, see Figs. 4(a) and 4(b).

The rich nature of the system means that further classification of the different solution types and the physical interpretation of the experimental results is facilitated by a suitable conceptual framework. We believe that two-dimensional capillary statics calculations can provide such a framework, and the arguments supporting this belief and details of the calculations are described in Sec. IV.

IV. THE ROLE OF TWO-DIMENSIONAL CAPILLARY STATICS

The experiments and previous numerical calculations[2,6] show that for non-oscillatory fingers, the interface becomes axially uniform within a few tube widths of the tip and the liquid is then effectively at rest.[13] Thus, the finger cross-section sufficiently far behind the tip must be a two-dimensional static equilibrium: i.e., the curvature of the cross-section in the wetted regions is equal to the pressure difference across the interface divided by the surface tension—the Young–Laplace equation. The external liquid pressure, and hence the interfacial curvature, is set by the dynamics near the finger tip, but the set of possible finger cross-sections can be computed by determining the realisable static equilibria in each tube geometry.

The possible interfacial cross-sections can be found by solving the two-dimensional Young–Laplace equation, subject to the constraints that the interface encloses a given area and that it meets the walls at a prescribed contact angle. We set the contact angle to zero because in our experiments the oil fully wets the tube walls. The remaining problem is then how to determine the enclosed area for a given capillary number. The area can be calculated directly from the experimental wet fraction m (the cross-sectional area of the air finger is $1 - m$ multiplied by the cross-sectional area of the tube), but a theoretical prediction of the area requires full three-dimensional simulations to resolve the near-tip dynamics. In the static limit ($Ca = 0$), however, there are no viscous forces and the pressure in the liquid is hydrostatic. Thus, the enclosed area, or equivalently the interfacial curvature, can be calculated directly from an axial force balance over a control volume.[8–10] A schematic is shown in Fig. 5 and the total pressure difference, Δp, over the finger tip must be balanced by the surface tension, σ, acting along the entire projected perimeter of the finger in a cross-section taken behind the tip. The contribution from the unwetted parts of the cross-section arises from the contact line where the finger tip meets the wall at zero contact angle. The argument is identical to the standard balance of forces on a hemi-spherical bubble demonstrating that Δp is given by $2\sigma/R$, where R is

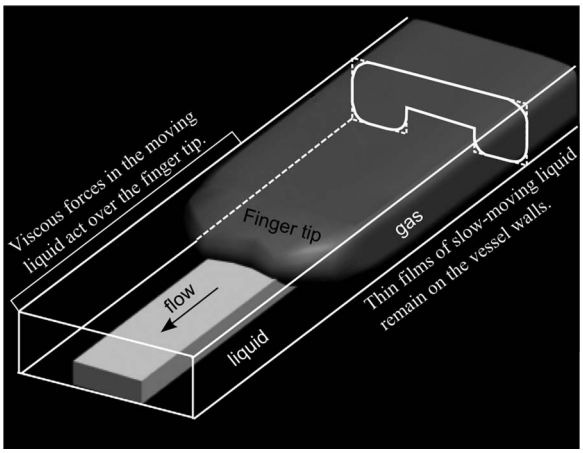

FIG. 5. Schematic of a three-dimensional air finger propagating from right to left in an axially uniform tube with a partially occluded rectangular cross-section. Behind the finger tip, the finger becomes axially uniform and an illustrative cross-section is shown in white. The remaining thin liquid films are essentially at rest and the majority of the viscous stress on the interface occurs near the tip region.

the radius of the hemisphere (Ref. 14, pp. 13–14). Thus, the force balance is given by

$$\iint \Delta p \, \mathrm{d}A = \oint \sigma \, \mathrm{d}s, \tag{1}$$

where the surface and line integrals are over the projected area and projected perimeter of the finger, respectively. As shown by Concus and Finn[8] and in detail by de Lazzer *et al.*,[9] Eq. (1) can also be derived by formal integration of the three-dimensional Young–Laplace equation.

We define a cross-sectional Cartesian (x^*, y^*) coordinate system such that gravity acts in the negative y^* direction and the origin of the coordinate system is on the centreline of the tube, see Fig. 6(a). We choose the (constant) air pressure as our reference pressure and set it to zero, so that the pressure difference across the interface is

$$\Delta p = \sigma \kappa_0^* + \rho g y^*, \tag{2}$$

where κ_0^* is the dimensional notional curvature of the interface on the midline of the cross-section, when $y^* = 0$. Using Eq. (2) in the integral force balance (1) gives

$$\iint \left(\sigma \kappa_0^* + \rho g y^*\right) \mathrm{d}A = \oint \sigma \, \mathrm{d}s, \tag{3}$$

and assuming that $\sigma \neq 0$ is a constant, we obtain the equation

$$\kappa_0^* \mathcal{A}^* + \frac{\rho g}{\sigma} \int y^* \, \mathrm{d}A = \mathcal{P}^*, \tag{4}$$

where $\mathcal{A}^*$ is the dimensional projected area and $\mathcal{P}^*$ is the dimensional perimeter of the interface within the cross-section. Non-dimensionalising based on the tube half-height $H/2$ and using Green's

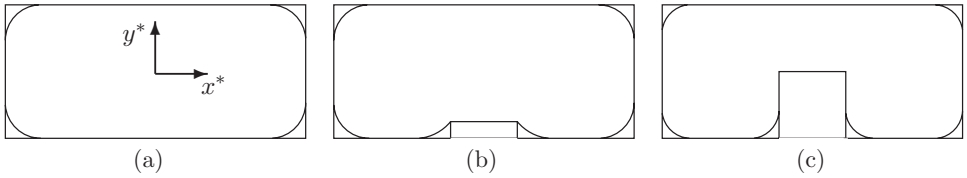

FIG. 6. Sketches of symmetric static equilibria in tubes of rectangular cross-section in the absence of gravity: (a) unoccluded, (b) low occlusion, and (c) high occlusion.

theorem in the plane gives

$$\mathcal{P} = \kappa_0 \mathcal{A} - Bo \oint \frac{y^2}{2} \mathrm{d}x, \tag{5}$$

where $\mathcal{P} = \mathcal{P}^*/(H/2)$, $\kappa_0 = (H/2)\kappa_0^*$, $(x, y) = (x^*/(H/2), y^*/(H/2))$, and $\mathcal{A} = \mathcal{A}^*/(H/2)^2$ are the equivalent dimensionless quantities.

For $Bo > 0$, solutions to the Young–Laplace equation subject to the constraint (5) must be computed numerically. In the absence of gravity, however, the pressure difference across the interface is constant, which means that when not in contact with the wall, the interface must be of constant curvature and the static solutions can be determined analytically. The constraint (5) becomes

$$\mathcal{P} = \kappa_0 \mathcal{A}, \tag{6}$$

and each interface section is either a straight line in contact with the tube wall or the arc of a circle with radius $1/\kappa_0$.

In unoccluded rectangular cross-sections the only possible static equilibrium that satisfies (6) consists of four quarter circles in the corners of the tube,[10] see Fig. 6(a). If the unit length is chosen to be the half-height of the rectangular cross-section, the radius of curvature, $\mathcal{R}$, of the static equilibrium is given by

$$\mathcal{R} = \frac{2(1+\alpha) - 2\sqrt{(1+\alpha)^2 + \alpha(\pi - 4)}}{4 - \pi}. \tag{7}$$

When a partial occlusion is introduced into the cross-section, the solution must be modified by the introduction of two circular arcs that meet the obstacle, see Fig. 6(b). The presence of the obstacle increases the available perimeter, but decreases the area, which means that the interface curvature must increase and it does so monotonically with increasing obstacle height. As the curvature increases, the two arcs evolve towards quarter circles, after which the upper part of the obstacle side wall becomes dry, see Fig. 6(c), but the curvature continues to increase monotonically with obstacle height.

In addition to modifying the symmetric solution as described above, the introduction of a partial occlusion allows alternative asymmetric static equilibria for sufficiently high obstacles, see Fig. 7. If the obstacle height is exactly equal to the tube height, then each side branch is an independent rectangular tube with static equilibrium given by Eq. (7), but with α replaced by the half-width of the side branch. These localised asymmetric equilibria may easily be obtained experimentally by introducing air on only one side of the obstacle. If the obstacle height is nearly equal to the channel height the asymmetric state will remain unchanged, see Fig. 7(a), until the gap above the obstacle exceeds the radius of curvature and the arc can no longer meet the side of the obstacle at zero contact angle. Below this height, the equilibrium becomes three quarter circles and an arc of a circle that is pinned on the corner of the obstacle, see Fig. 7(b). As the height of the obstacle is reduced further, the pinned arc evolves smoothly from a quarter circle, meeting the side of the obstacle, to a semi-circle that meets the top of the obstacle when $\alpha_h = \alpha_h^c$, see Fig. 7(c). In this configuration, the curvature is set by the gap width above the obstacle and there is a degeneracy in the solution because it costs nothing energetically to extend the infinitesimal film above the obstacle. This expansion of the finger over the obstacle allows the smooth transition from localised to non-localised asymmetric fingers. An alternative family of asymmetric solutions is possible in which the interface is pinned

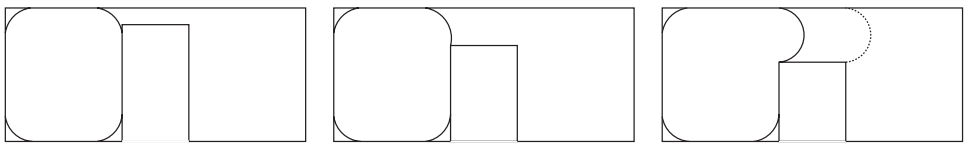

FIG. 7. Sketches of asymmetric static equilibria in tubes of rectangular cross-section in the absence of gravity: (a) high occlusion, (b) medium occlusion, and (c) low occlusion.

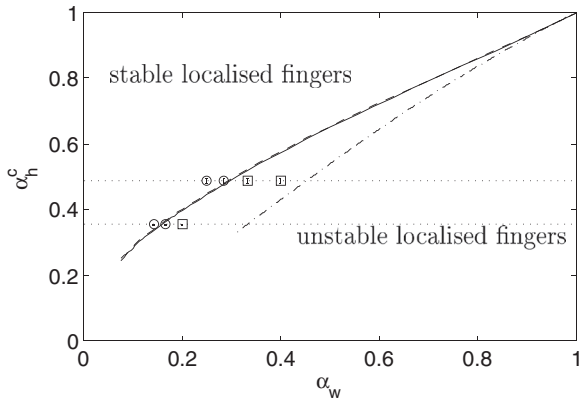

FIG. 8. Static prediction of the existence of asymmetric localised fingers in terms of the relative obstacle size α_h and α_w. The experimental tube had $H = 3.07 \pm 0.01$ mm and $Bo = 1.058 \pm 0.008$. The solid line shows SE computations for $H = 3.06 \pm 0.01$ mm and $Bo = 1.050$, while the almost indistinguishable dashed line is for $H = 3.08 \pm 0.01$ mm and $Bo = 1.065$. Circles indicate tube geometries where localised fingers are stable when the flow is suddenly stopped ($Ca = 0$), while squares correspond to tubes where localised fingers are unstable at $Ca = 0$. The dotted-dashed line is the analytic prediction in the absence of gravity ($Bo = 0$) corresponding to Eq. (A6).

to the opposite side of the obstacle, see the dashed line in Fig. 7(c), but again these solutions only exist for $\alpha_h > \alpha_h^c$. The two solution branches coincide at $\alpha_h = \alpha_h^c$ (other possible solutions are precluded on physical grounds because the interface passes through the wall). Thus, we conclude that an asymmetric solution at $Ca = 0$ is only possible for $\alpha_h > \alpha_h^c$. Note that an alternative family of symmetric solutions is also possible in which there are two disconnected localised fingers, one in each side-channel, provided that the obstacle is sufficiently wide that their interfaces do not intersect. Details of the explicit calculation of α_h^c are presented in the Appendix and the result is shown in Fig. 8.

A. Comparison between static experiments and static simulations: $Ca = 0$

The presence of gravity does not alter the overall picture, but does alter the quantitative details. In order to compare with experimental data, we performed two-dimensional Surface Evolver (SE)[15] calculations to solve the Young–Laplace equation subject to the constraint (5), which was enforced by using a Newton method. Figure 8 shows the computed critical curve delineating the region in which asymmetric localised solutions are predicted to exist in the static limit ($Ca = 0$) as a function of the parameters α_w and α_h^c. Note that in the calculations the interface was explicitly pinned to one corner of the obstacle. The prediction for α_h^c when $Bo = 0$ computed in the Appendix is also shown. Experimentally, we recorded the existence of a static localised finger if it remained localised for 5 min or more after arresting its propagation by switching off the flow. Experiments were performed for $\alpha_h = 0.49$ and 0.35, and successive tube widths were tested to determine the value of α_w at which static localised fingers were first observed. The quantitative agreement between experiments and calculations in Fig. 8, namely, that the computed line does divide the experimentally observed stable and unstable localised fingers, suggests that a two-dimensional static model of the cross-section of the finger is sufficient to predict the state of the three-dimensional finger at $Ca = 0$, at least on intermediate timescales. On long timescales, modification of the finger can occur due to end effects and the Rayleigh–Taylor and Rayleigh–Plateau instabilities.[16] As described above, tall obstacles promote the existence of localised states and the small gap width above the obstacle means that gravitational effects are not significant. However, as the width of the side-channels increases relative to the obstacle width, i.e., as α_w decreases, localised fingers are found for decreasing obstacle heights. The same trend is found in the absence of gravity and arises because, for the critical configuration, an increase in width of the side-channel leads to a more rapid increase in projected area than perimeter of the finger. This necessitates a decrease in curvature, and therefore a decrease in obstacle height is

TABLE I. Wet fractions at $Ca = 0$ computed using SE corresponding to the experimental data for $\alpha_h = 0.49$ presented in Fig. 3. The experimental values correspond to straight line extrapolation of the two data points with smallest Ca to the value $Ca = 0$.

	Wet fraction			
	Symmetric solution		Asymmetric localised solution	
α_w	Experiment	Calculation	Experiment	Calculation
2/5	0.17	0.17	...	...
1/3	0.13	0.14	...	...
2/7	0.11	0.11	...	...
1/4	0.11	0.10	0.60	0.60
1/5	0.09	0.09	0.59	0.59
1/8	0.07	0.07	0.56	0.56

required in order to maintain the force balance. For non-negligible gravitational forces, the projected area is smaller and increases less rapidly, which is why the critical obstacle height remains greater than that when $Bo = 0$.

In addition to predictions of the existence of asymmetric solutions at $Ca = 0$, we can make further quantitative comparison between the experiments and static simulations by comparing the wet fractions for symmetric and asymmetric localised solutions. In the experiments, we employ a linear extrapolation of the two data points with smallest Ca to the value $Ca = 0$, while in the simulations the wet fraction is equal to the fractional area of the cross-section unoccupied by the air finger, see Table I. The results are in excellent agreement with the experimental data. The general trend of decrease in wet fraction with increasing tube width is because the additional side-channel area is predominantly occupied by the air finger.

B. Comparison between experimental data and static simulations: $Ca > 0$

In the simulations, having established the possible $Ca = 0$ solutions, the action of viscous forces can be included by relaxing the constraint (5) and modifying the cross-sectional area of the finger, which is a function of Ca. The exact relationship between capillary number and area must be determined from the experiments, but we have found that enclosed area can serve as a reasonable proxy for Ca. For non-zero Ca the additional viscous stresses that act on the finger tip must be included in the force balance, and can be accommodated by increasing the total pressure difference (air pressure minus fluid pressure) across the interface, or by reducing the contribution of surface tension by reducing the perimeter of the finger's cross-section.

For the symmetric solutions, both mechanisms lead to an increase in the finger tip curvature, which ultimately reduces the projected area and hence the wet fraction increases with increasing Ca, as confirmed by experimental data, see Fig. 3. The evolution of the symmetric solution with increasing Ca is therefore approximated by starting from the appropriate $Ca = 0$ solution, reducing the enclosed area, and computing the corresponding solutions of the Young–Laplace equation.

For initially localised asymmetric solutions, in addition to increasing the finger tip curvature, the finger could expand over the obstacle to increase the projected area and therefore the total pressure drop, although this will also increase the cross-sectional perimeter and may also increase the total viscous force. Expansion of the interface over the obstacle allows the continuous transition from localised to non-localised asymmetric fingers described above and explains the decrease in wet fraction observed experimentally, see Fig. 3. For the widest tube $\alpha_w = 1/8$, it appears to be favourable to reduce the finger tip curvature before expansion of the interface leading to an initial increase in wet fraction. In other words, the behaviour of the localised solutions will be the same as the symmetric solutions (curvature increasing with Ca) until the transverse interfacial curvature is large enough that the interface can expand over the obstacle without further increase in curvature.

We conducted further Surface Evolver calculations to establish the validity of the proposed two-dimensional approach. The capillary number is not a governing parameter in the simulations, so

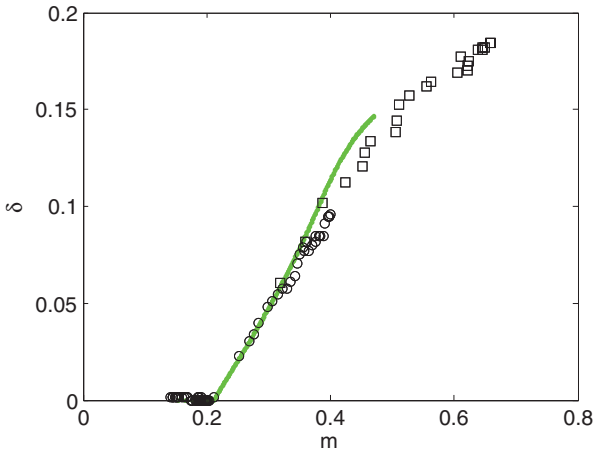

FIG. 9. Comparison between two-dimensional SE calculations of cross-sectional finger shapes and experiments for $\alpha_h = 0.35$ and $\alpha_w = 1/3$. Experimental results were obtained with silicone oils of different dynamic viscosities: circles $\mu = 4.81 \times 10^{-3}$ kg m^{-1}s^{-1} and squares $\mu = 9.7 \times 10^{-2}$ kg m^{-1}s^{-1}. The two-dimensional static solutions, shown as the solid line (green), are in excellent agreement with the experiments, suggesting that the loss of stability of the symmetric finger can be predicted from existence of the non-localised asymmetric state that forms behind the finger tip in the SE calculations. The value of δ was measured at a distance of 45 mm behind the finger tip.

we parameterise the two-dimensional solutions and experimental data by the wet fraction, m, and the finger offset, δ, defined in Sec. II and Fig. 2. Results for two different obstacle heights are presented in Figs. 9 and 10. In both cases, the experimental data are in good agreement with the two-dimensional calculations, confirming that the experimental results can be captured by the two-dimensional static model. We reiterate, however, that we can neither determine the capillary numbers nor whether the solutions are experimentally realised without experimental data. Nonetheless, having established the mapping between the experimental data and static solutions, the static calculations reveal the approximate cross-sections of each finger.

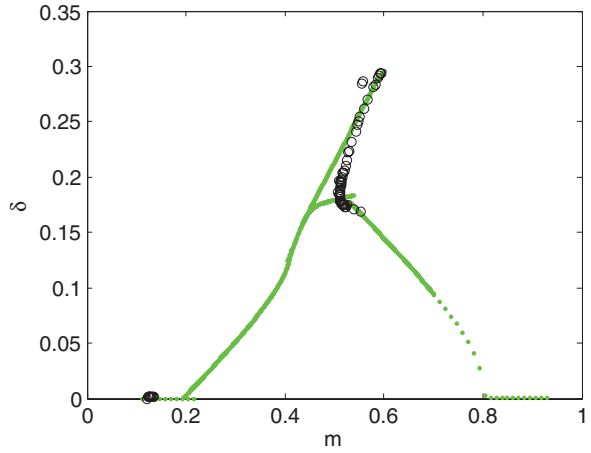

FIG. 10. Comparison between two-dimensional SE calculations of cross-sectional finger shapes and experiments for $\alpha_h = 0.49$ and $\alpha_w = 1/4$. Experimental results (circles) were obtained with silicone oil of dynamic viscosity $\mu = 4.81 \times 10^{-3}$ kg m^{-1}s^{-1}. The localised solution occurs at the point $m \approx 0.6$, $\delta \approx 0.3$ and is predicted accurately by the static calculations (solid line and dots, green). The broadening of the finger is qualitatively captured by the static calculations, with good agreement once the finger is detached from both side walls, but the exact details of the evolution are different in the simulations and experiments. The value of δ was measured at a distance of 45 mm behind the finger tip.

C. Criteria for bifurcation

The model presented can predict the existence of solutions at $Ca = 0$ and is consistent with the experimental data at $Ca > 0$. Thus, we hope to be able to extract information about the bifurcation by using additional insight from the static simulations. In Fig. 9 (low obstacle $\alpha_h = 0.35$), the bifurcation appears to be supercritical and the loss of symmetry in the experimental data is in excellent agreement with the loss of symmetry in the equivalent static calculations. In Fig. 10 (high obstacle $\alpha_h = 0.49$), however, the bifurcation is subcritical and the experimental symmetric solution loses stability before (at lower m than) the static symmetric solution. The static solution becomes degenerate when it loses symmetry and leaves the side walls because it may move to different locations within the cross-section without changing its curvature, area, or perimeter. The loss of stability of the physical system at this point of static degeneracy is not surprising; we would expect an alternative non-degenerate solution to be selected, if such a solution is available. We believe that the loss of static stability provides an upper bound for the bifurcation point, but that a dynamic mechanism leads to bifurcation at lower values of the wet fraction (capillary number) in the majority of cases. For example, in Fig. 10 the maximum experimental wet fraction for symmetric fingers, $m \approx 0.12$, is considerably lower than the point at which the simulation first becomes asymmetric, $m \approx 0.2$. As the width of the tube increases, α_w decreases and the length of the region along which the finger meets the side wall at $Ca = 0$ decreases, which means that a smaller increase in wet fraction (and we infer Ca) is required before the static stability is lost. The physical bifurcation must therefore also occur at lower Ca, as observed in the experiments.

D. Regions of finger oscillations

The oscillatory dynamics cannot be captured in our model because axial variations are neglected. However, if the mechanism proposed by Pailha *et al.*[7] is correct then the asymmetric state of widest extent (minimum wet fraction) that will not induce dynamic oscillations of the interface is that where the interface extends over, but not beyond, the entire obstacle. We use Surface Evolver to calculate such asymmetric configurations in the experimental geometries used in Fig. 3. The initial configuration is chosen to be analogous to the asymmetric non-localised $Ca = 0$ state of minimum curvature where one side wall has a dry region and the interface is pinned at the far edge of the obstacle, see Fig. 7(c). The enclosed volume is adjusted until the angle between the interface and the upper surface of the obstacle is less than 1° and the solution is iterated until its length changes by less than a given tolerance, typically 10^{-4}, although validation was performed by using smaller tolerances. The corresponding wet fractions are presented in Table II and are accurate to two decimal places.

The simulation results demonstrate that the wet fractions of the proposed limiting steady asymmetric solutions increase with decreasing α_w, albeit very slowly. (The difference between the values for $\alpha_w = 2/5$ and $\alpha_w = 1/3$ is in the third decimal place.) The computed wet fractions are within 10% of the experimental data, suggesting that the form of the static solution is correct for $\alpha_w \geq 2/7$, when there is no asymmetric solution at $Ca = 0$. That said, there is no clear trend in the experimental

TABLE II. Wet fractions computed using SE for the proposed limiting steady asymmetric fingers for different tube widths corresponding to the experimental data presented in Fig. 3. The experimental values correspond to the steady (non-oscillatory) asymmetric solution with minimum wet fraction. Note that when $\alpha_w = 2/7$ the data point with $m = 0.33$ is not chosen because it is believed to correspond to an oscillatory solution.

	Minimum steady asymmetric wet fraction	
α_w	Computed	Experimental
2/5	0.42	0.44
1/3	0.42	0.46
2/7	0.43	0.42

data, which may be due to localised pinning of the interface away from the very edge of the obstacle. We also investigated the cases when there is an asymmetric solution at $Ca = 0$ ($\alpha_w < 2/7$). Here, the computed wet fractions are systematically lower than those found experimentally and we infer that the form of the static solutions is no longer appropriate. Indeed, re-inspection of Fig. 4 reveals that the oscillatory fingers at $\alpha_w = 1/3$ meet both side walls, but at $\alpha_w = 1/8$ the finger does not meet either side wall, a qualitative difference between the states.

V. CONCLUSIONS

We have presented results from an experimental study of two-phase displacement flows in axially uniform tubes of partially occluded rectangular cross-section. The results demonstrate that for sufficiently high occlusions two alternative stable solutions are possible for low capillary numbers: a steadily propagating symmetric air finger that spans the majority of the tube or a steadily propagating asymmetric air finger localised within one of the side-channels. However, the detailed understanding of the effects of initial conditions on the finger configuration would require a separate study.

For a given occlusion height, if the tube is sufficiently wide, the bistable behaviour persists to the limit of zero capillary number, when the fluid is at rest. We compute solutions to the two-dimensional Young–Laplace equations augmented by an axial force balance to predict the region of existence of the localised asymmetric solutions at zero capillary number and the results are in excellent agreement with the experimental data. The computations reveal that asymmetric solutions arise because the interface can either meet the side of the obstacle or localise on the edge of its upper surface. The calculations also predict that an alternative symmetric solution consisting of two localised fingers, one in each side-channel, is also possible. Such a solution has not been sought experimentally in the rigid geometries, but similar double-tipped fingers have been observed in two-phase displacement flows in elastic tubes.[17]

By using the enclosed area as a proxy for capillary number, the experimental results can be mapped to the two-dimensional solutions of the Young–Laplace equation, which reveals the approximate transverse cross-section of the interface far behind the finger tip. We deduce that an upper limit for bifurcation from the symmetric state is given by the wet fraction at which the finger no longer meets the side walls of the tube and becomes statically degenerate. If the bifurcation occurs at this point it will be supercritical, otherwise it will be subcritical and is induced by an unknown dynamic mechanism. Nonetheless, the movement of the experimentally observed bifurcation to smaller values of Ca with increasing tube width is explained by the decrease in wet fraction at which the symmetric static state leaves the wall in the solutions of the Young–Laplace equation.

The two-dimensional computations are only appropriate for cases in which there are no axial oscillations of the interface, but the results are consistent with the mechanism for the onset oscillation proposed in Ref. 7. The mechanism is driven by the change in transverse curvature induced when the interface passes laterally over one edge of the occlusion. Computation of steady asymmetric states that extend over the entire occlusion, but not beyond it, give wet fractions that are within 10% of the minimum steady asymmetric wet fractions found in the experiments when there are no asymmetric localised solutions at $Ca = 0$.

We believe that the surprisingly rich dynamics of the system is entirely a consequence of the existence of non-degenerate asymmetric static solutions. The occlusion provides a distinguished location within the cross-section that can remove translational degeneracy from the continuum of quasi-two-dimensional asymmetric solutions. Symmetry breaking has also previously been observed in two-phase displacement flows in cylindrical tubes[18] and Hele-Shaw cells,[19] when the interface is perturbed by the introduction of wires within the tube. In those cases, rather than introducing a new family of asymmetric static solutions, local modification of the finger tip where it is penetrated by the wire selects a particular asymmetric solution from the existing continuum.

The introduction of additional static solutions by modification of the tube geometry may be of use in geometry-based control of microfluidic systems. The capillary static calculations presented above demonstrate that the mechanism is independent of gravity, so would still apply in microchannels. In fact, we have observed transitions to asymmetric and oscillatory fingers and bubbles in preliminary microchannel experiments. Thus, local changes in flow rate induced by global changes in channel

dimension coupled to localised geometric features could be used to direct bubbles and droplets based on their volume, physical properties, and local propagation speeds. Naturally, we would expect the system to exhibit different responses to trains rather than individual bubbles and droplets, but the existence of additional modes of propagation, and therefore the ability to switch between them, would remain.

The system is somewhat unusual from a fluid mechanical point of view, because multiple stable solutions exist at zero flow. That multiple solutions can exist is, of course, a consequence of the presence of the air-liquid interface which introduces nonlinearity into the system. The specific details of the solution structure and evolution of the bifurcation diagram with changes in parameters is not fully understood. However, we believe that the most important difference from the unoccluded tube is an increase in transverse curvature in the occluded region and would expect that the majority of the features of the system will be present in a Hele-Shaw model with a spatially variable permeability; such a model is the subject of a current investigation.

ACKNOWLEDGMENTS

We thank the Engineering and Physical Sciences Research Council (EPSRC) for support through Grant No. EP/H011579/1 (M.P.) and Advanced Research Fellowships (A.J. and S.J.C.).

APPENDIX: CALCULATION OF α_h^c IN THE ABSENCE OF GRAVITY

For the configuration shown in Fig. 11, we note immediately that the configuration is not possible unless the height of the channel is large enough to accommodate the semi-circular meniscus in the narrow section **and** the quarter-circular meniscus in the left-hand lobe. Thus,

$$2 \geq 3(1-\alpha_h^c) \quad \Rightarrow \quad 2 \geq 3 - 3\alpha_h^c \quad \Rightarrow \quad 3\alpha_h^c \geq 1 \quad \Rightarrow \quad \alpha_h^c \geq \frac{1}{3},$$

and we obtain a lower bound for α_h^c. An upper bound follows from the trivial observation that the step-height must be less than the entire height of the channel, $\alpha_h^c < 1$, so the proposed solutions are only possible if

$$\frac{1}{3} \leq \alpha_h^c < 1. \tag{A1}$$

In this configuration the curvature is set by the height of the obstacle and is given by $\kappa_0 = 1/(1-\alpha_h^c)$. Hence, the total projected perimeter of the finger is

$$\mathcal{P} = \frac{5}{2}\pi(1-\alpha_h^c) + 4\mathcal{L} + 2\alpha(1-\alpha_w) - 4(1-\alpha_h^c) + 4\alpha_h^c, \tag{A2}$$

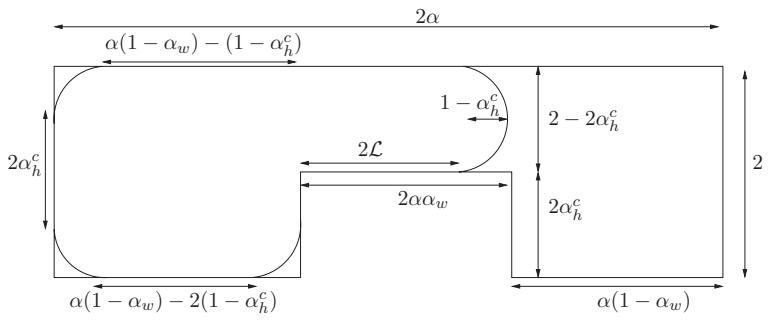

FIG. 11. The geometry of an asymmetric static bubble with maximum curvature in a tube with partially occluded cross-section. The half-height of the channel is chosen to be the reference length-scale and is set to 1.

and the projected area is

$$\mathcal{A} = \frac{5}{4}\pi(1-\alpha_h^c)^2 + 4\mathcal{L}(1-\alpha_h^c) + 2\alpha_h^c\alpha(1-\alpha_w) + [2\alpha(1-\alpha_w) - 3(1-\alpha_h^c)](1-\alpha_h^c). \quad \text{(A3)}$$

Using Eqs. (A2) and (A3) and the relationship between κ_0 and α_h^c in the constraint (6) gives

$$\frac{5}{2}\pi(1-\alpha_h^c) + 4\mathcal{L} + 2\alpha(1-\alpha_w) - 4(1-\alpha_h^c) + 4\alpha_h^c =$$

$$\frac{5}{4}\pi(1-\alpha_h^c) + 4\mathcal{L} + \frac{2\alpha_h^c\alpha(1-\alpha_w)}{1-\alpha_h^c} + 2\alpha(1-\alpha_w) - 3(1-\alpha_h^c). \quad \text{(A4)}$$

The immediate cancellation of the factor of $4\mathcal{L}$ from both sides indicates that, if it exists, the solution is degenerate because the semi-circular arc can be placed anywhere within the narrow section without changing the surface energy. Equation (A4) is a quadratic equation for α_h^c, which has the solution

$$\alpha_h^c = \frac{6 - (5/2)\pi - 2\alpha(1-\alpha_w) \pm \sqrt{[2\alpha(1-\alpha_w) + (5/2)\pi - 6]^2 - (20-5\pi)(1-(5/4)\pi)}}{(10-(5/2)\pi)}. \quad \text{(A5)}$$

Hence, α_h^c varies as a function of the dimensionless side-channel width $\alpha(1-\alpha_w) = (W-w)/H$. In our experiments, the width of the obstacle is kept constant and is three times the height of the tube, so $(W-w)/H = (3/2)(1/\alpha_w - 1)$ and Eq. (A5) becomes

$$\alpha_h^c = \frac{6 - (5/2)\pi - 3(1/\alpha_w - 1) \pm \sqrt{[3(1/\alpha_w - 1) + (5/2)\pi - 6]^2 - (20-5\pi)(1-(5/4)\pi)}}{(10-(5/2)\pi)}. \quad \text{(A6)}$$

The (positive) solution branch is plotted as the dotted-dashed line in Fig. 7. The solution decreases monotonically with increasing side-channel width, as also found in the Surface Evolver calculations with gravity. Solutions of this form are only possible for $0 < \alpha(1-\alpha_w) \leq 3.28$. For wider side-channels, the configuration fully wets the side wall of the obstacle, but a slightly modified calculation demonstrates that α_h^c continues to decrease with increasing side-channel width.

[1] G. I. Taylor, "Deposition of viscous fluid on the wall of a tube," J. Fluid Mech. **10**, 161–165 (1961).
[2] A. L. Hazel and M. Heil, "The steady propagation of a semi-infinite bubble into a tube of elliptical or rectangular cross-section," J. Fluid Mech. **470**, 91–114 (2002).
[3] C. Clanet, P. Hérault, and G. Searby, "On the motion of bubbles in vertical tubes of arbitrary cross-sections: some complements to the Dumitrescu–Taylor problem," J. Fluid Mech. **519**, 359–376 (2004).
[4] C. Hollis, V. Vahrenkamp, S. Tull, A. Mookerjee, C. Taberner, and Y. Huang, "Pore system characterisation in heterogeneous carbonates: an alternative approach to widely used rock-typing methodologies," Mar. Pet. Geol. **27**, 772–793 (2010).
[5] M. Heil, A. L. Hazel, and J. A. Smith, "The mechanics of airway closure," Respir. Physiol. Neurbiol. **163**, 214–221 (2008).
[6] A. de Lózar, A. Heap, F. Box, A. L. Hazel, and A. Juel, "Partially-occluded tubes can force switch-like transitions in the behavior of propagating bubbles," Phys. Fluids **21**, 101702 (2009).
[7] M. Pailha, A. L. Hazel, P. A. Glendinning, and A. Juel, "Oscillatory bubbles induced by geometric constraint," Phys. Fluids **24**, 021702 (2012).
[8] P. Concus and R. Finn, "On the behaviour of a capillary surface in a wedge," Proc. Natl. Acad. Sci. U.S.A. **63**(2), 292–299 (1969).
[9] A. de Lazzer, D. Langbein, M. Dreyer, and H. J. Rath, "Mean curvature of liquid surfaces in cylindrical containers of arbitrary cross-section," Microgravity Sci. Technol. **9**, 208–219 (1996).
[10] H. Wong, C. J. Radke, and S. Morris, "The motion of long bubbles in polygonal capillaries. Part 1. Thin films," J. Fluid Mech. **292**, 71–94 (1995).
[11] F. P. Bretherton, "The motion of long bubbles in tubes," J. Fluid Mech. **10**, 166–188 (1961).
[12] A. de Lózar, A. L. Hazel, and A. Juel, "Scaling properties of coating flows in rectangular channels," Phys. Rev. Lett. **99**, 234501 (2007).
[13] We note that immeasurably small draining flows will persist over very long timescales until rupture of the thin liquid films deposited on the wall.
[14] C. Isenberg, *The Science of Soap Films and Soap Bubbles* (Dover Publications Inc., New York, 1992).
[15] K. Brakke, "The Surface Evolver," Exp. Math. **1**, 141–165 (1992).
[16] M. Fermigier, L. Limat, J. E. Wesfreid, P. Boudinet, and C. Quilliet, "Two-dimensional patterns in Rayleigh–Taylor instability in a thin layer," J. Fluid Mech. **236**, 349–383 (1992).
[17] A. Heap and A. Juel, "Anomalous bubble propagation in elastic tubes," Phys. Fluids **20**, 081702 (2008).
[18] R. M. Fearn, "Perturbed motions of a bubble rising in a vertical tube," Phys. Fluids **31**, 238–241 (1988).
[19] G. Zocchi, B. E. Shaw, A. Libchaber, and L. P. Kadanoff, "Finger narrowing under local perturbations in the Saffman–Taylor problem," Phys. Rev. A **36**, 1894–1900 (1987).